ChemPubSoc Europe

DOI: 10.1002/cctc.201200408

Oxidative Coupling of Methane by Nanofiber Catalysts

Daniel Noon, Anusorn Seubsai, and Selim Senkan*[a]

The direct utilization of methane, the main component in natural gas (NG), as an alternate chemical feedstock to petroleum is a highly desirable but difficult goal in industrial catalysis.[1] Many direct and indirect methods have been proposed and studied to convert CH_4 into more-useful products, including olefins (e.g. C_2H_4, C_3H_6) and higher-molecular-weight hydrocarbons and liquids (e.g. benzene and gasoline), as discussed in a recent review.[1] The production of ethylene (C_2H_4) from NG represents a particularly desirable process because of its massive worldwide use as an intermediate in the production of plastics, such as polyethylene and polyvinylchloride (PVC). In addition, ethylene can be oligomerized into liquid hydrocarbons, thereby enabling the efficient utilization of natural gas in remote parts of the world. The global production rate of ethylene is over 100 million tons per year, which represents an annual business in excess of $110 billion (July 2012). All indirect NG-conversion routes utilize a high temperature, endothermic, and costly steam-reforming process as the first step, from which synthetic gas (H_2/CO mixtures) is produced. This step is followed by the synthesis of useful products through various catalytic processes.[1] Although direct methods avoid the use of costly syngas, they remain uneconomical, owing, in part, to low yields of C_{2+} compounds, high temperatures, and low throughputs. High temperatures are particularly detrimental because they result in catalyst deactivation and create problems for reactors.

In the oxidative coupling of methane (OCM), CH_4 is directly converted into C_2H_6, C_2H_4, and water in the presence of O_2 and a suitable catalyst.[1] The first step involves the abstraction of H from CH_4 by the catalyst to form methyl radicals ($CH_3^{\bullet}$).[2,3] The coupling of two $CH_3^{\bullet}$ radicals creates C_2H_6, followed by its dehydrogenation to afford C_2H_4. Some C_3 hydrocarbons are also formed by the addition of a $CH_3^{\bullet}$ radical to C_2H_4.[4] However, undesirable surface reactions and gas-phase combustion reactions also lead to CO and CO_2 (CO_x). Because high temperatures promote homogeneous gas-phase free-radical reactions, which are detrimental for C_{2+} products, the development of new catalysts that can operate at low temperatures is crucial for the economic viability of the OCM.

Since the pioneering works of Keller and Bhasin,[5] Hinsen and Baerns,[6] and Ito and Lunsford,[7] the OCM has received immense global attention, as evidenced by the large number of catalysts that have been investigated for this transformation:[2] The oxides of almost all of the metals on the periodic table, either individually or in various combinations, have been considered and analyzed as OCM catalysts.[2] Even the best catalysts have been reported to require feed-gas temperatures (T_f) of 700–850 °C and reaction times of 0.2–5.5 s, with C_{2+} yields of less than 25 %.[2] Gas temperatures within the catalytic zones were found to be 100–200 °C higher than this range, owing to the exothermicity of this process.[8] The actual catalyst-surface temperature is likely to be even higher still because of heat-transfer considerations. An important common feature of all of these OCM catalysts is that they are based on quasi-spherical nanoparticles (powders)[1,2] and, thus, are prone to metal dispersion, agglomeration, and sintering. All of these problems retard catalytic activity. Herein, we report a new fabric catalyst that is comprised of La_2O_3–CeO_2 nanofibers; this catalyst is capable of negating these problems and promoting the ignition of the OCM at a T_f value of 470 °C. The nanofibers were prepared by electrospinning. An analogous La_2O_3–CeO_2 powder catalyst was also prepared by co-precipitation for comparison. Powders of this binary system have previously been studied by Dedov et al.[9] and have been reported to show OCM activity at significantly higher T_f values (715–830 °C).

Shown in Figure 1 (left) is the calcined La_2O_3–CeO_2 nanofiber fabric (La/Ce, 15:1 w/w) that was used in the OCM experiments. A SEM image of this fabric (Figure 1, right) shows the formation of highly uniform La_2O_3–CeO_2 nanofibers with diameters in the range 50–75 nm. This fabric had a low BET area of about 26 $m^2 g^{-1}$, which suggested that the nanofibers were dense and did not possess any internal porosity. The SEM image also shows the presence of large voids between the fibers, which enhances fabric diffusivity and decreases sintering.

The XRD data for La_2O_3–CeO_2 nanofibers and powders, both before and after the test conditions, are presented in Figure 2 (A, B and C, D), along with those for individual La_2O_3 (E) and CeO_2 (F) fibers and powders. From these data, several interesting features are revealed: First, both the La_2O_3 fibers (Fig-

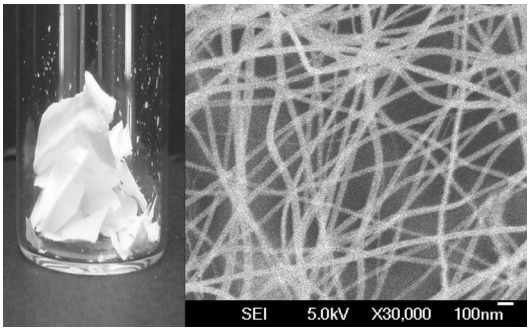

Figure 1. La_2O_3–CeO_2 fabric catalyst (left) and its SEM image (right).

[a] D. Noon, Dr. A. Seubsai, Prof. Dr. S. Senkan
University of California, Los Angeles
Department of Chemical Engineering
Los Angeles, CA 90095-1592 (USA)
Fax: (+1) 310-440-8309
E-mail: ssenkan@gmail.com

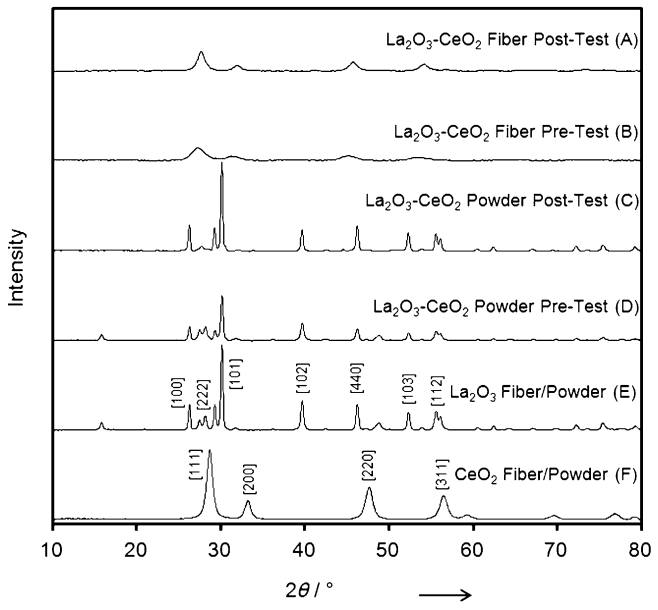

Figure 2. Comparison of the XRD spectra of La_2O_3–CeO_2 nanofibers with those of related materials.

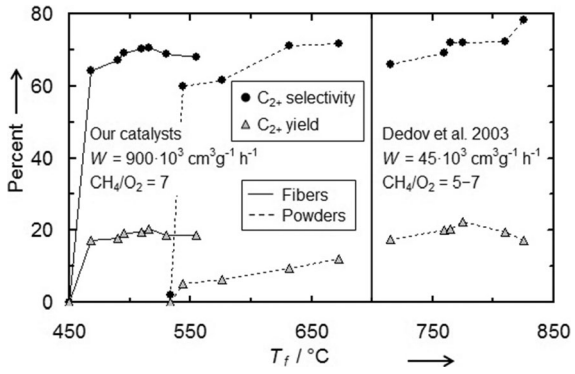

Figure 3. Left: Comparison of the OCM results with the La_2O_3–CeO_2 fabric catalyst to those with co-precipitated powders at the same gas-throughput value (*W*). Right: Previous powder studies by Dedov et al.[9] at a 20× lower *W* value.

ure 2E) and powders exhibit almost-identical mixed cubic (222 and 440 reflections) and hexagonal structures (100, 101, and 102 reflections).[10] Similarly, the same cubic (111, 200, and 220 reflections) CeO_2 phases were present in both the fibers and the powder.[11] However, the XRD spectrum of binary La_2O_3–CeO_2 nanofibers showed that they were remarkably less crystalline than the La_2O_3 and CeO_2 fibers (Figure 2B). This result can be attributed to the formation of solid solutions and the reactions of La_2O_3 and CeO_2, such as the partial reduction of ceria into Ce_7O_{12} and the incorporation of La^{3+} ions into the cubic lattice of CeO_2.[9,12] Significant shortening and broadening of the La_2O_3–CeO_2 nanofiber peaks are also shown, thus indicating smaller mean crystallite dimensions compared to single metal-oxide nanofibers.

Second, the diffractograms of the La_2O_3–CeO_2 nanofibers were substantially different to those of the co-precipitated powders at the same La/Ce weight ratio (15:1). Most interestingly, although the La_2O_3–CeO_2 nanofibers were less crystalline (Figure 2B), the powders exhibited reflections that were characteristic of crystalline phases (Figure 2D) and remained as such, even after the OCM experiments (Figure 2C). Third, the post-test XRD peaks for the nanofibers were slightly sharper, thus suggesting some increase in crystallite size. Lastly, the La_2O_3–CeO_2 nanofibers exhibited a number of new peaks (indicated by *) that were not present in either the powders or in in the single metal-oxide fibers. Clearly, further characterization is required for to develop a better understanding of the active sites in the binary La_2O_3–CeO_2 nanofibers and to further improve their OCM performances.

OCM experiments with La_2O_3–CeO_2 fabrics were also conducted by using a microreactor and compared to co-precipitated powders with the same La/Ce weight ratio (15:1). Feed-gas compositions were kept between 80–87.5 mol% CH_4 and 12.5–20 mol% O_2, which corresponded to CH_4/O_2 ratios of 7:1 to 4:1. The feed-gas throughput (*W*) was about 900×10^3 $cm^3\,h^{-1}$ per gram of catalyst. In Figure 3, the results of the nanofiber experiments are compared to powders at a CH_4/O_2 ratio of 7:1.

The percentage selectivities for C_{2+} products and yields (C_{2+} selectivity from the conversion of CH_4) are presented as a function of feed-gas temperature (T_f). As shown in Figure 3, the La_2O_3–CeO_2 nanofibers exhibited OCM ignition at $T_f \approx 470\,^{\circ}C$, concomitant with an 18% yield of C_{2+} compounds and 65% C_{2+} selectivity. Thermocouple measurements in the reactor tube, in the direction of the gas flow, indicated a sharp increase in temperature to a maximum value (T_{rx}) of about 630 °C within the catalytic zone, which represents a temperature rise of 160 °C, owing to the OCM. The temperature immediately started to decrease at the downstream quartz wool plug and reached the furnace temperature within 10–15 mm. As shown in Figure 3, an increase in T_f increased the C_{2+} yield and selectivity to 20% and 70% respectively, peaking at 520 °C ($T_{rx} \approx 670\,^{\circ}C$).

Under identical conditions, the performance of our La_2O_3–CeO_2 powders was significantly different. The powders ignited at a higher feed temperature of 540 °C, with an initial C_{2+} yield of only 5% and a C_{2+} selectivity of 60%. However, with increasing T_f value, both C_{2+} selectivity and yield increased steadily. At $T_f \approx 630\,^{\circ}C$, the C_{2+} yield and selectivity were 9% and 70%, respectively.

The yield and selectivity of C_{2+} products that were reported by Dedov et al.[9] for their La_2O_3–CeO_2 powder catalysts by using a similar packed-bed reactor are also shown in Figure 3, right, albeit at a significantly lower gas throughput ($W = 45\times10^3$ $cm^3\,h^{-1}$ per gram of catalyst). As shown in Figure 3, substantially higher feed-gas temperatures, in the range 715–830 °C, were required to achieve C_{2+} yields and selectivities that were similar to those of our nanofiber catalysts. Also, notably, even at the lower gas throughputs used by Dedov et al., higher catalyst-bed temperatures (in excess of 900 °C) would still be expected, based on the axial temperature profiles reported in OCM reactors under similar *W* values and CH_4/O_2 ratios at comparable CH_4 conversions and C_{2+} selectivities.[8]

In all of our experiments, O_2 conversions were near or above 90% after ignition. Also, the La_2O_3–CeO_2 fabrics did not exhibit an apparent deactivation or change in selectivity, even after longer-term experiments (>10 h). OCM studies with pure La_2O_3 nanofibers without the CeO_2 dopant produced inferior results.

We believe that the increased OCM performance that is offered by the fabrics reported herein warrants more-detailed studies to better understand the underlying physical and chemical processes that are responsible for these results. In addition to thorough characterization, an exploration of the effects of the diameter of these nanofibers, the La/Ce ratio, and space time on the OCM will provide important new insight into this nanofiber catalysis. Although nanofibers provide excellent metal dispersion and easy access to the catalytic sites, their high performance could also be related to different crystal facets that are exposed compared to particles, as reported previously in an entirely different system.[13] The XRD results (Figure 2) also support this conclusion as a distinct possibility.

The OCM results for the same La_2O_3–CeO_2 fabric catalyst are presented for a CH_4/O_2 feed ratio of 4 (Figure 4). Here, the

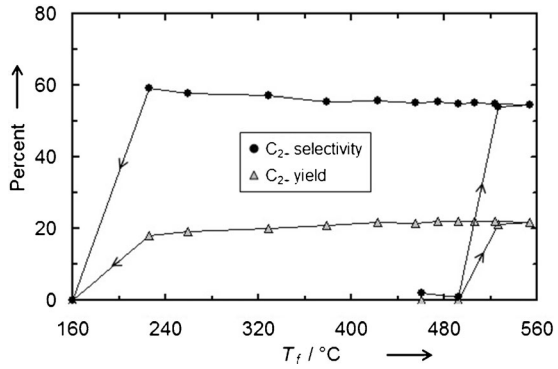

Figure 4. OCM results with the La_2O_3–CeO_2 fabric catalyst at a CH_4/O_2 feed ratio of 4 and a throughput of $W = 900 \times 10^3$ cm^3 g^{-1} h^{-1}.

onset of catalyst ignition was at 520 °C on increasing the T_f value, with a C_{2+} selectivity of 55% and a yield of 22%. However, a remarkably broad hysteresis window was noted. In Figure 4, on decreasing the T_f value, the high performance of the La_2O_3–CeO_2 nanofibers was shown to extend down to a quench of $T_f \approx 230$ °C, thus indicating an autothermal T_f range of 290 °C (i.e. 520–230 °C).

In summary, fabrics of metal-oxide nanofibers represent a new class of high-performance catalytic materials with potential applications in industrial chemistry. By providing excellent dispersion, order, and access to the catalytic sites, La_2O_3–CeO_2 fabrics exhibited high OCM performance at significantly lower feed-gas temperatures (T_f) than analogous powder catalysts. These nanofiber fabrics also exhibited large voids, which should enhance diffusivity and decrease sintering.

Experimental Section

La_2O_3–CeO_2 nanofibers were prepared by electrospinning.[14] In a typical experiment, the metal precursor (0.15 g), as $La(NO_3)_3 \cdot 6H_2O$ and $Ce(NO_3)_3 \cdot 6H_2O$, and polyvinylpyrrolidone (PVP, 0.40 g, 1.3 MDa) were added to a water/EtOH mixture (1:1 w/w, 9.5 g). Upon complete mixing, the solution was loaded into a syringe, which was placed into a syringe pump. The syringe was connected to a metal needle and a DC voltage (30 kV) was applied that caused the nanofibers to be ejected towards a grounded collector that was 15 cm away. The electrospun material was calcined at 625 °C in a furnace to form metal-oxide nanofiber fabrics. The La/Ce weight ratio was about 15. An analogous La_2O_3/CeO_2 powder catalyst was also prepared for comparison. This powder was synthesized by simply mixing the aforementioned metal-nitrate precursors at the same ratio in water, followed by evaporation over a hot plate to precipitate out the powders and subsequent calcination at 625 °C. Notably, the OCM performance of the La_2O_3–CeO_2 nanofibers was extremely sensitive to the preparation and storage conditions.

The nanofiber and powder catalysts (8 mg) were packed into a 4 mm ID quartz tube, sandwiched between two quartz wool plugs, and placed inside a temperature-controlled tube furnace. The reactor pressure was 1 atm. The inlet gas-flow rates were regulated at 120 cm^3 min^{-1} by electronic mass-flow controllers (MKS). These conditions corresponded to a feed-gas throughput of 900 10^3 cm^3 h^{-1} per gram of catalyst (5–10 ms contact time). The gas compositions were maintained between 80–87.5 mol% CH_4 and 12.5–20 mol% O_2. The reaction products were sampled by using a small amount of glass-lined tubing and analyzed by on-line gas chromatography (Varian 4900 Micro-GC, with Molecular sieve X and Porapak U columns). The reactor temperature was changed incrementally and, after each temperature had settled, the outlet-gas composition was determined. The temperature in the furnace was measured by a thermocouple that was placed in the upstream of the reactor. A thermocouple (diameter: 0.25 mm) was also placed immediately after the catalyst to determine the temperature of the reaction products.

Characterization of the catalysts was performed by powder X-ray diffraction (PANalytical X'Pert PRO that was fitted with a Ni filter and a Soller slit collimator). CuK_α radiation (45 kV, 40 mA) was used to identify the active catalyst phases. BET surface areas were determined on Quantachrome Autosorb-1 units with a micropore-analysis option. SEM images were obtained on a JEOL JSM-67 Field-Emission Scanning Electron Microscope.

Acknowledgements

We thank B. Zohour for his assistance in some of the experiments. We also thank the LCS for the use of their facilities and database. D.N. acknowledges the NSF (MCTP-DGE-0654431).

Keywords: cerium · heterogeneous catalysis · lanthanum · nanostructures · oxidation

[1] M. C. Alvarez-Galvan, N. Mota, M. Ojeda, S. Rojas, R. M. Navarro, J. L. G. Fierro, *Catal. Today* **2011**, *171*, 15 – 23.
[2] U. Zavyalova, M. Holena, R. Schlögl, M. Baerns, *ChemCatChem* **2011**, *3*, 1935 – 1947.
[3] J. H. Lunsford, *Angew. Chem.* **1995**, *107*, 1059 – 1070; *Angew. Chem. Int. Ed. Engl.* **1995**, *34*, 970 – 980.
[4] S. J. Conway, D. J. Wang, J. H. Lunsford, *Appl. Catal. A* **1991**, *79*, L1 – L5.

[5] G. E. Keller, M. M. Bhasin, *J. Catal.* **1982**, *73*, 9 – 19.
[6] W. Hinsen, M. Baerns, *Chem. Ztg.* **1983**, *107*, 223.
[7] T. Ito, J. H. Lunsford, *Nature* **1985**, *314*, 721 – 722.
[8] S. Pak, J. H. Lunsford, *Appl. Catal. A* **1998**, *168*, 131 – 137.
[9] A. G. Dedov, A. S. Loktev, I. I. Moiseev, A. Aboukais, J.-F. Lamonier, I. N. Filimonov, *Appl. Catal. A* **2003**, *245*, 209 – 220.
[10] N. Imanaka, T. Masui, Y. Kato, *J. Solid State Chem.* **2005**, *178*, 395 – 398.
[11] C. Hu, Z. Zhang, H. Liu, P. Gao, Z. Lin Wang, *Nanotechnology* **2006**, *17*, 5983 – 5987.
[12] X. Cao, R. Vassen, W. Fischer, F. Tietz, W. Jungen, D. Stöver, *Adv. Mater.* **2003**, *15*, 1438 – 1442.
[13] a) P. Christopher, S. Linic, *J. Am. Chem. Soc.* **2008**, *130*, 11264 – 11265; b) S. Linic, P. Christopher, *ChemCatChem* **2010**, *2*, 1061 – 1063.
[14] S. Tan, X. Huang, B. Wu, *Polym. Int.* **2007**, *56*, 1330 – 1339.

Received: June 25, 2012
Revised: September 5, 2012
Published online on December 3, 2012